Kinetics of $ClONO_2$ Reactive Uptake on Ice Surfaces at Temperatures of the Upper Troposphere

Miguel A. Fernandez,[†] Robert G. Hynes,[‡] and Richard A. Cox*,[†]

Centre for Atmospheric Science, Department of Chemistry, University of Cambridge, CB2 1EW, United Kingdom, and CSIRO Energy Technology, Lucas Heights Science and Technology Centre, PMB 7, Bangor, NSW 2234, Australia

Received: June 27, 2005; In Final Form: August 16, 2005

The reactive uptake kinetics of $ClONO_2$ on pure and doped water−ice surfaces have been studied using a coated wall flow tube reactor coupled to an electron impact mass spectrometer. Experiments have been conducted on frozen film ice surfaces in the temperature range 208−228 K with $P_{ClONO_2} \leq 10^{-6}$ Torr. The uptake coefficient (γ) of $ClONO_2$ on pure ice was time dependent with a maximum value of $\gamma_{max} \sim 0.1$. On HNO_3-doped ice at 218 K the γ_{max} was 0.02. HOCl formation was detected in both experiments. On HCl-doped ice, uptake was gas-phase diffusion limited ($\gamma > 0.1$) and gas-phase Cl_2 was formed. The uptake of HCl on ice continuously doped with HNO_3 was reversible such that there was no net uptake of HCl once the equilibrium surface coverage was established. The data were well described by a single site 2-species competitive Langmuir adsorption isotherm. The surface coverage of HCl on HNO_3-doped ice was an order of magnitude lower than on bare ice for a given temperature and P_{HCl}. $ClONO_2$ uptake on this HCl/HNO_3-doped ice was studied as a function of P_{HCl}. γ_{max} was no longer gas-phase diffusion limited and was found to be linearly dependent on the surface concentration of HCl. Under conditions of low HCl surface concentration, hydrolysis of $ClONO_2$ and reaction with HCl were competing such that both Cl_2 and HOCl were formed. A numerical model was used to simulate the experimental results and to aid in the parametrization of $ClONO_2$ reactivity on cirrus ice clouds in the upper troposphere.

Introduction

Chlorine activating reactions on ice surfaces have been a major focus of laboratory experiments since it was suggested they play an important role in the depletion of stratospheric ozone during the Antarctic spring. Since then, laboratory studies[1−8] have revealed that the heterogeneous reactions R1 and R2 proceed very efficiently on the surface of polar stratospheric clouds (PSC) at temperatures of the polar stratosphere ($T < 200$ K).

$$ClONO_2 + H_2O \rightarrow HOCl + HNO_3 \qquad (R1)$$

$$ClONO_2 + HCl \rightarrow Cl_2 + HNO_3 \qquad (R2)$$

There is now emerging evidence that these reactions can occur on the surface of ice particles in cirrus clouds at the warmer temperatures, typically 205−230 K, of the Upper Troposphere (UT). The potential for cirrus clouds to play a role in chlorine activation in the UT was first suggested by Borrmann[9] and later by Solomon et al.[10] Raman Lidar measurements of the UT which showed ozone minima in the presence of ice cloud layers[11] may be explained by heterogeneous chlorine activation on cirrus ice clouds. Indeed, model calculations using kinetic data applicable to the colder temperatures of the polar stratosphere have shown that up to 50% activation of reservoir chlorine on cirrus may be possible.[10,12] Observations of enhanced ClO concentrations during cirrus events in the tropopause region support the link between observed low ozone and chlorine activation on cirrus.[13,14] Model calculations suggest that the elevated ClO concentrations could significantly increase ozone loss in this region.[13]

The model calculations carried out to date have relied on relatively simple parametrizations of heterogeneous reaction kinetics using uptake coefficients for ice surfaces recommended by the NASA panel for data evaluation.[15] The recommendation gives single, temperature-independent, values of the rate determining uptake coefficients, which are based mainly on experiments conducted under conditions relevant for polar stratospheric clouds consisting of water ice or solid nitric acid trihydrate at $T < 200$ K.[2−4,6,7,16] There is now evidence from laboratory studies that at higher temperatures appropriate for cirrus clouds, the reactivity of the ice surface is lower and the uptake coefficients are more strongly temperature dependent.[6,17−22] In addition, we have shown that when multiple species are simultaneously present (i.e., HNO_3 and HCl), there is competition for adsorption sites which can affect heterogeneous reaction rates. It is therefore important to understand the dependence of heterogeneous reaction rates on the surface coverage of the reactants. This would be a useful tool in differentiating between Langmuir−Hinshelwood and Eley−Rideal surface reaction mechanisms and thus aid in the parametrization of rate constants in models.

Parametrization of reaction rates for varying conditions of temperature, humidity, and reactant partial pressures using surface coadsorption models has been described by Tabazedah and Turco[23] and Carslaw and Peter.[24] These models have been used by these groups to examine the available laboratory data for the reaction of HCl with HOCl and $ClONO_2$ on ice and

* Corresponding author. E-mail: rac26@cam.ac.uk. Phone: (+44) 1223-336-253. Fax: (+44) 1223-336-362.
[†] University of Cambridge.
[‡] Lucas Heights Science and Technology Centre.

10.1021/jp053477b CCC: $30.25
Published on Web 10/15/2005

NAT within the framework of a coadsorption model. This analysis revealed large discrepancies in the experimental data but enabled a parametrization for the reaction rates for NAT at $T < 210$ K and calculations of polar ozone loss.[24] The discrepancies preclude any meaningful extrapolation of reaction rate parameters to cirrus cloud temperatures and knowledge of the rate coefficients for chlorine activating reactions in the upper troposphere remains highly uncertain.

To address this uncertainty we have measured the reaction probabilities of $ClONO_2$ on a variety of ice surfaces at temperatures relevant to upper tropospheric cirrus clouds and parametrized the reactivity in terms of the above-mentioned coadsorption models.

Experimental Methods

The Coated Wall Flow Tube. Experiments were carried out in a double-jacketed cylindrical flow tube reactor coupled to an electron impact quadrupole mass spectrometer (Hiden Analytical model HAL IV) described in detail previously.[25] The system has recently been reorientated from a vertical to a horizontal configuration, which has allowed an improved protocol for ice film preparation to be used. In addition, the mass spectrometer has been upgraded to digital electronics with pulse counting capabilities and simultaneous multispecies monitoring. The detection limit for $ClONO_2$, monitored at mass 46 (NO_2^+ fragment), was $\sim 4 \times 10^{-8}$ Torr for S/N =1.

Ice films were prepared by establishing a uniform film of liquid water on the inner surface of a Pyrex sleeve. This was then inserted into the flow tube reactor precooled to 258 K. The Pyrex sleeve was rotated constantly during this procedure to ensure that an even ice film was formed throughout the length of the tube and to minimize large variations in film thickness. The flow reactor was then cooled to the required temperature: 208, 218, or 228 K. The water used was high purity (Acros Organics; >99.99% purity). Ice films were maintained during the course of an experiment by the addition of a co-flow of helium saturated with water. This was achieved by bubbling 100 sccm of helium through a reservoir of pure water at a fixed temperature. The water-saturated flow of helium was then passed through a Pyrex spiral to remove supersaturated droplets prior to entering the flow tube. The ice film thickness was calculated using the volume of water used (measured accurately with a pipet and kept constant between experiments), the density of ice, and the inner surface area of the Pyrex insert. This calculation yields an ice film thickness of ~ 100 μm.

Reactant gases were exposed to a known length of ice using a Pyrex sliding injector positioned along the central axis of the flow tube reactor. Flow meters were used to deliver a known flow rate of reactant into the reactor. The helium carrier gas was fixed at 400 sccm and controlled with a mass flow controller. The total pressure inside the reactor was $\sim 1.70-1.80$ Torr with a total flow velocity of ~ 1500 cm s^{-1}.

Preparation of Chemicals. $ClONO_2$ was prepared by reacting N_2O_5 with Cl_2O. N_2O_5 was prepared by reaction of excess O_3 with NO (MG Gases, 99.99%). Ozone was produced by passing a flow of oxygen (BOC high purity) through a high-voltage commercial ozonizer. White crystals of N_2O_5 were collected in a coldfinger at dry ice temperatures. Cl_2O was prepared by passing pure Cl_2 (MG Gases, 99.99%) over yellow mercury(II) oxide (Sigma-Aldrich >99.0%) in a Pyrex u-tube. Cl_2O appeared as a cherry red liquid at dry ice temperatures. The Cl_2O sample was then purified by trap-to-trap distillation to remove excess Cl_2 and transferred to the N_2O_5 sample vial. This was left overnight in a cryogenic acetone/dry ice bath to completely react. Purification of $ClONO_2$ samples was carried out to remove the impurities, Cl_2, and unreacted N_2O_5. This was done by trap-to-trap distillation at 173 K (methanol and liquid N_2) versus 77 K (liquid N_2) to remove the Cl_2, and again at 195 K (dry ice/acetone slush) versus 77 K to remove any unreacted N_2O_5. The purity of $ClONO_2$ samples used in experiments was determined by UV−vis spectrometry and found to be >95% pure (the main impurity was Cl_2). Gas dilutions of $ClONO_2$ in high-purity helium were prepared prior to every experiment and stored in a 10 L blackened Pyrex mixing bulb. HCl gas mixtures were prepared in mixing bulbs by diluting HCl (Messer Gases; >99.8% purity) in high-purity helium. Gaseous HNO_3 was prepared prior to each experiment by reacting sulfuric acid (96 wt %) with HNO_3 (67 wt %). The gaseous HNO_3 was cryo-trapped at 77 K and then subjected to several freeze−pump−thaw cycles before some condensed HNO_3 was allowed to evaporate into a blackened Pyrex mixing bulb and diluted with high-purity helium. The uncertainty in the mixing ratios of the reactants in the storage bulbs was $\sim$25%.

Measurement Procedures. Experiments conducted on surfaces doped with HNO_3 and/or HCl required the use of a 2 mm i.d. Teflon tube located at the upstream end of the ice surface such that a continuous flow of dopant could be delivered to the ice surface. Under these conditions the entire ice surface was continuously doped and the sliding injector was always downstream of the Teflon tube such that only doped ice was exposed to the reactant gas stream from the injector. In this study, partial pressures of HNO_3 were maintained at 1×10^{-6} Torr such that at the temperatures employed and water vapor partial pressures present, the NAT stability region of the HNO_3-H_2O phase diagram was avoided. Similarly, to avoid the hydrate region of the $HCl-H_2O$ phase diagram, partial pressures of HCl employed were below 2×10^{-6} Torr. Mass spectrometer signals were calibrated for each of the reactant species (HCl, $ClONO_2$, and HNO_3) before every experiment. In each case the mass spectrometer signals were found to be linearly dependent on the partial pressure of the reactant. HCl was monitored at m/z 36. Both $ClONO_2$ and HNO_3 were monitored at m/z 46. The mass spectrometer response at m/z 46 was more sensitive to $ClONO_2$ by $\sim$35% so changes in the relative amounts of these gases present together could be monitored but with reduced sensitivity. To distinguish the initial $ClONO_2$ signal from the HNO_3 signal at m/z 46, it was necessary to introduce the gases in sequence and subtract one signal from the other. After exposure of $ClONO_2$ to the ice surface, the NO_2^+ signal contains contributions from both the $ClONO_2$ and any desorbed HNO_3 produced in the surface reaction and provides only qualitative indications of $ClONO_2$ concentration changes. The products Cl_2 (m/z 70) and HOCl (m/z 52) were also calibrated. HOCl was calibrated indirectly by using the relative magnitude of the change in $ClONO_2$ and HOCl signals for $ClONO_2$ + ice experiments during the initial stages of the uptake where subsaturation quantities of HNO_3 were formed on the surface which did not desorb and contaminate the NO_2^+ signal. Desorption of HNO_3 has been observed from saturated ice surfaces at 218 K but no net desorption was found at subsaturation coverages ($<3 \times 10^{14}$ molecules cm^{-2}).[21,26]

Results

HCl Uptake on HNO_3-Doped Ice. In these experiments, we extended our previously reported results[21] for the uptake of HCl on HNO_3-doped ice to cover a wider range of P_{HCl} at three temperatures (208, 218, 228 K). Our previous results at 218 K and $P_{HCl} = (0.5-1.5) \times 10^{-6}$ Torr showed that (1) HCl surface

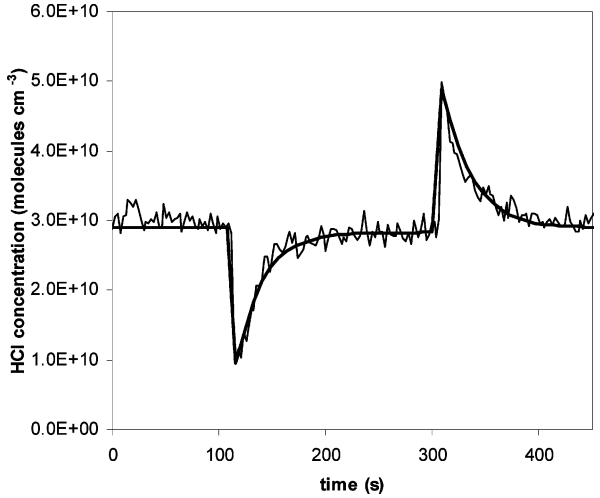

Figure 1. HCl uptake ([HCl] = 3×10^{10} molecules cm^{-3}) on HNO_3-doped ice at 218 K. The HCl gas stream is exposed to 6.8 cm of ice between $t = 100$ and 300 s. The surface coverage of HCl after exposure is $\sim 5.6 \times 10^{13}$ molecules cm^{-2}. The smooth black line is the model fit to the experimental data.

coverage, θ, increased with P_{HCl} and, compared to the uptake on "bare" ice, is reduced by approximately an order of magnitude for a given P_{HCl} in the above range; (2) the uptake was, within experimental uncertainty, completely reversible such that the HCl adsorbed on exposing the ice surface to the HCl gas stream was equal to the HCl desorbed when the injector was returned to the zero position and exposure of the HCl gas flow to the surface ceased; and (3) the surface coverage dependence at low P_{HCl} can be adequately modeled by using a Langmuir adsorption isotherm for single site adsorption.

Figure 1 shows a typical uptake profile of HCl on a surface saturated with HNO_3 at 218 K. The sliding injector was withdrawn to expose the ice surface to the HCl gas stream at 100 s and returned to the zero position at 300 s. The amount of HCl desorbed was equal to that adsorbed within experimental uncertainty.

Parts a, b, and c of Figure 2 show adsorption isotherms for HCl uptake on HNO_3-doped ice surfaces at 208, 218, and 228 K, respectively, with $P_{HCl} = (0.3-4) \times 10^{-6}$ Torr. In each case the entire ice surface was continually exposed to HNO_3 ($P_{HNO_3} \sim 1.0 \times 10^{-6}$ Torr). The amounts of adsorbed HCl were calculated by integrating the signal from the initial drop in signal until the point where the signal recovers to a steady level. The surface coverage was then calculated by using the geometric surface area of the ice exposed, the total flow rate, the integrated signal area, and a calibration for the HCl signal. At 218 and 228 K, the P_{HNO_3} and P_{H_2O} in this study were such that ice was the thermodynamically favorable phase in the HNO_3-H_2O phase diagram. However, at 208 K the experimental conditions were in a region of the phase diagram close to the supercooled liquid coexistence line within the NAT region. The possibility of "surface melting" may lead to larger time-dependent uptakes observed by both ourselves and other groups.[27] Nevertheless, the HCl adsorption was reversible under these conditions. The solid lines in Figure 2 represent Langmuir fits to the experimental data using a single site 2-species competitive adsorption model. It was assumed that the maximum surface coverage (θ_{max}) of both HNO_3 and HCl was 3×10^{14} molecules cm^{-2} at all temperatures. This assumption is supported by numerous studies[17,28,29] which suggest that the θ_{max} of a number of different species on ice tends toward 3×10^{14} molecules cm^{-2}. The Langmuir equation for competitive

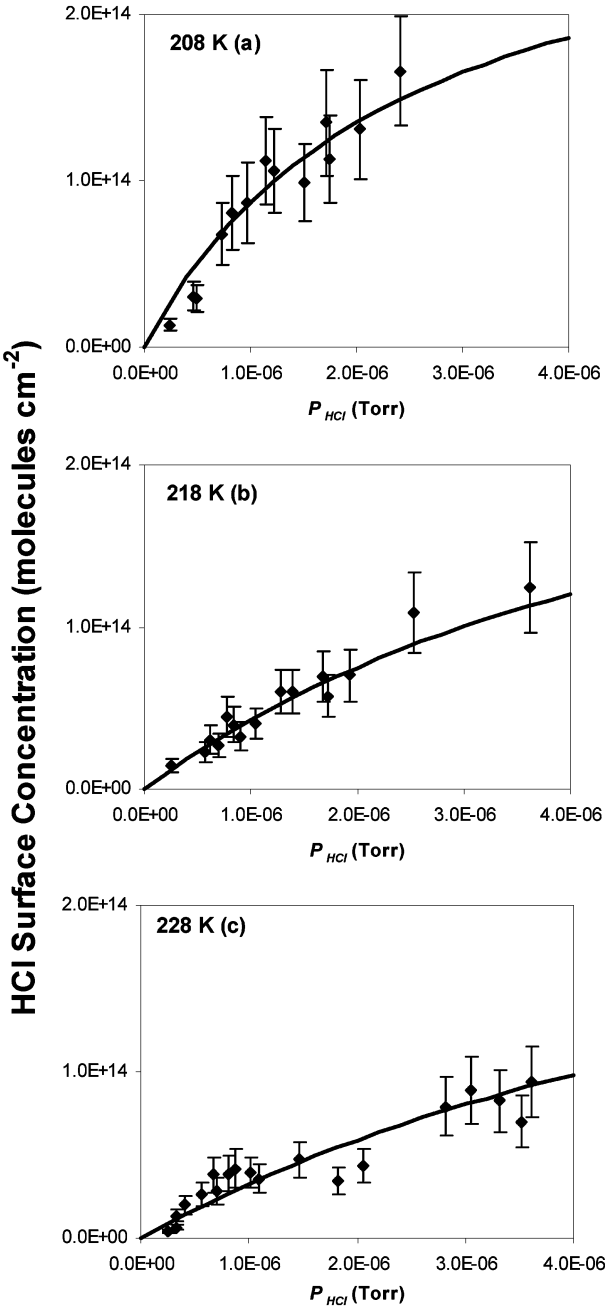

Figure 2. Adsorption isotherms for HCl uptake on HNO_3-doped ice at (a) 208, (b) 218, and (c) 228K. Solid lines are best fits to a Langmuir single site model with competitive adsorption between HNO_3 and HCl.

adsorption is given below in eq 1:

$$\theta_{HCl} = \frac{[HCl]_{ads}}{\theta_{max}} = \frac{[HCl]_g K_{eq}^{HCl}}{1 + [HCl]_g K_{eq}^{HCl} + [HNO_3]_g K_{eq}^{HNO_3}} \quad (1)$$

where $[HCl]_{ads}$ is the concentration of adsorbed HCl molecules (molecules cm^{-2}), $[HCl]_g$ is the gas-phase concentration of HCl (molecules cm^{-3}), $[HNO_3]_g$ is the gas-phase concentration of HNO_3 (molecules cm^{-3}), and K_{eq} is the Langmuir equilibrium constant for HCl or HNO_3 (cm^3 molecule^{-1}).

The data in Figure 2 were well represented by eq 1. $K_{eq}^{HNO_3}$ values were taken from a separate publication,[30] which describes the application of a numerical model to fit the HNO_3-ice experimental data of Ullerstam et al.[26] These K_{eq} values are considerably higher than our earlier determination[21] by fitting

TABLE 1: Equilibrium Constants for HCl and HNO_3

temp/K	K_{eq}(HCl)/cm^3 molecule^{-1}	K_{eq}(HNO_3)/cm^3 molecule^{-1}
208	$(1.8 \pm 0.1) \times 10^{-10}$	$(4.3 \pm 0.4) \times 10^{-10}$
218	$(5.6 \pm 0.4) \times 10^{-11}$	$(3.2 \pm 0.2) \times 10^{-10}$
228	$(2.6 \pm 0.2) \times 10^{-11}$	$(1.9 \pm 0.02) \times 10^{-10}$

with a dissociative Langmuir model. K_{eq}^{HCl} was determined from our experimental data by fitting eq 1 to the isotherms in Figure 2. The K_{eq} values for both HNO_3 and HCl are presented in Table 1. The K_{eq} values were used together with the gas-phase HCl concentration to calculate the HCl surface coverage in $ClONO_2$ + HCl experiments which follow.

$ClONO_2$ Reactive Uptake on Bare and HNO_3-Doped Ice Surfaces. Figure 3 shows an uptake experiment for exposure of a 10 cm long bare ice film to $ClONO_2$ at 218 K ($P_{ClONO_2} = 6.2 \times 10^{-7}$ Torr). The ice was exposed to the $ClONO_2$ gas stream between $t = 250$ and 860 s. Initially, the NO_2^+ signal level dropped very sharply and was accompanied by an increase in the $HOCl^+$ (m/z 52) signal, which peaked after ~60 s. The NO_2^+ signal then recovered to a value lower than the initial signal indicating that some $ClONO_2$ was continuously lost by reaction to form HOCl at the ice surface and this is reflected in the $HOCl^+$ signal. The time-dependent component of the HOCl production ($t = 250-400$ s) is attributed to the partial deactivation of the ice surface by adsorbed HNO_3, a product of the surface reaction between $ClONO_2$ and H_2O. The nature of the HNO_3 surface deactivation is not known but it is likely that the presence of strongly adsorbed HNO_3 reduces the number of available surface water molecules, thus reducing the number of sites at which $ClONO_2$ can react. In addition, HNO_3 may be blocking sites for $ClONO_2$ adsorption prior to reaction with H_2O. Under conditions of continuous HOCl production ($t = 400-860$ s) a steady state supply of reactive sites maintains a constant reactive uptake coefficient for $ClONO_2$ and therefore a constant rate of HOCl production. The sliding injector was returned to the zero position at $t = 860$ s at which point the NO_2^+ signal temporarily exceeded the initial signal level. This apparent desorption signal can be attributed to HNO_3 or $ClONO_2$ desorbing from the surface. We have shown previously[21] that HNO_3 desorption occurs from ice surfaces which have a saturated surface coverage of HNO_3 of $\sim 3 \times 10^{14}$ molecules cm^{-2} at 218 K. At $t = 400$ s (Figure 3) sufficient $ClONO_2$ loss (i.e., $\sim 3 \times 10^{14}$ molecules cm^{-2}) had occurred to produce enough HNO_3 to saturate the surface. This corresponds to the point at which the HOCl production rate becomes constant. It follows that the NO_2^+ signal in Figure 3 cannot be used as a quantitative description of $ClONO_2$ uptake once a saturated surface coverage of HNO_3 has been attained. A mass balance of the apparent total $ClONO_2$ lost to the surface (as given by the NO_2^+ signal) versus the HOCl produced revealed less $ClONO_2$ lost than HOCl produced. This observation is explained by the contribution of HNO_3 desorption to the NO_2^+ signal during the latter stages of the uptake. However, mass balance was observed during the time-dependent portion of the HOCl production (i.e., $t = 250-400$ s). The HOCl is observed in the gas phase immediately upon exposure of the ice surface to the $ClONO_2$ gas stream, consistent with the known weak adsorption of HOCl on ice at temperatures above 155 K.[31,32] The rate of formation of HOCl peaked when the rate of decline of NO_2^+ was maximum and then fell to a constant rate. No other reaction products were observed in the gas phase.

The maximum (γ_{max}) and steady state (γ_{ss}) uptake coefficients for $ClONO_2$ uptake on bare ice were calculated by using the maximum drop in signal for γ_{max} and for γ_{ss}, the drop in signal once a stable and continuous uptake had been established. The rate constant (k) for removal of the reactant molecule from the gas phase was calculated by using these signal differences as shown in eq 2. The uptake coefficients were then obtained by using eq 3:

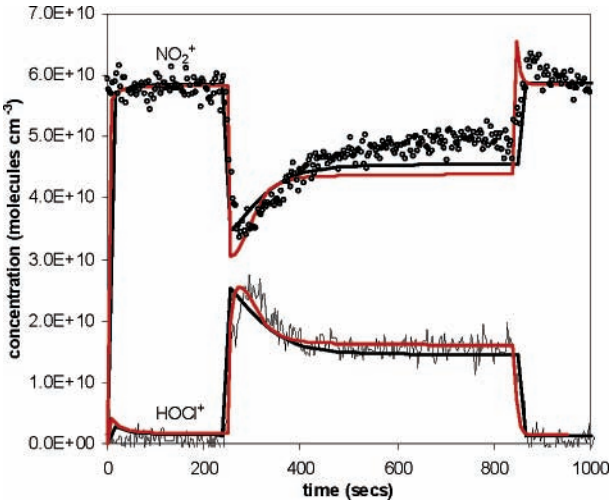

Figure 3. Uptake of $ClONO_2$ ($P_{ClONO_2} \sim 6.2 \times 10^{-7}$ Torr) on a "bare" ice surface at 218 K. Ice was exposed to $ClONO_2$ at $t = 250$ s and exposure was stopped at $t = 860$ s. NO_2^+ is shown by empty circles and $HOCl^+$ is represented by the noisy black line. The NO_2^+ signal has been offset by $+1 \times 10^{10}$ molecules cm^{-3} for clarity. The smooth line fits to the data represent model simulations for $ClONO_2$ and HOCl gas-phase concentrations with Eley−Rideal (black line) and Langmuir−Hinshelwood (red line) reaction mechanisms.

$$k = \frac{\nu}{z} \ln\left(\frac{S_{(0)}}{S_{(t)}}\right) \quad (2)$$

$$\gamma = \frac{2k'r}{\omega} \quad (3)$$

where ν is the flow velocity (cm s^{-1}), z is the length of ice exposed (cm), $S_{(0)}$ is the signal before exposure to the ice surface, and $S_{(t)}$ is the signal after time t. γ_{max} is calculated by taking $S_{(t)}$ to be the lowest signal value after exposure to the ice while γ_{ss} takes $S_{(t)}$ to be the signal during continuous uptake. k' refers to the value of k corrected for radial gas-phase diffusion,[33] r is the inner radius of the Pyrex sleeve (0.80 cm), and ω is the average molecular velocity of $ClONO_2$. The correction of the first-order rate constant for radial diffusion requires knowledge of the diffusion coefficient of $ClONO_2$ inside the flow tube, which was calculated by using the Chapman−Enskog formulation.[34] The pressure-independent diffusion coefficient of $ClONO_2$ was calculated to be ~110 cm^2 s^{-1} at 218 K and 1.7 Torr.

At 218 K and $P_{ClONO_2} = (0.3-1.2) \times 10^{-6}$ Torr, γ_{max} decreased with increasing P_{ClONO_2}, with values in the range 0.09 at 3×10^{-7} Torr to 0.025 at 1.2×10^{-6} Torr. Typical values of $\gamma_{ss} \sim 0.02$ were calculated with no discernible dependence on P_{ClONO_2}. These values are summarized in Table 2.

In a separate set of experiments, the ice surface was first doped with 1×10^{-6} Torr of HNO_3 until the ice surface was completely saturated. Saturated HNO_3 surface coverage was $\sim 2.4 \times 10^{14}$ molecules cm^{-2}.[21] Figure 4 shows a typical $ClONO_2$ ($P_{ClONO_2} \sim 7.0 \times 10^{-7}$ Torr) uptake experiment on HNO_3-doped ice at 218 K. The HOCl production rate reached a constant value without passing through the maximum, which was observed on an initially bare ice surface. Moreover, although HOCl appeared promptly in the gas phase it did not reach a

TABLE 2: Summary of Uptake Coefficients for $ClONO_2$ Reactive Uptake

reaction	temp/K	P_{ClONO_2}/Torr	γ
$ClONO_2$ + bare ice	218	3.3×10^{-7}	0.090 ± 0.025
	218	4.4×10^{-7}	0.065 ± 0.018
	218	5.2×10^{-7}	0.082 ± 0.033
	218	5.7×10^{-7}	0.069 ± 0.024
	218	6.2×10^{-7}	0.051 ± 0.018
	218	6.6×10^{-7}	0.069 ± 0.014
	218	1.1×10^{-6}	0.039 ± 0.006
	218	1.3×10^{-6}	0.024 ± 0.006
$ClONO_2$ + HNO_3-doped ice	218	7.0×10^{-7}	0.019 ± 0.006
	228	6.1×10^{-7}	0.009 ± 0.004
reaction	temp/K	P_{HCl}/Torr	γ
$ClONO_2$ + HCl-doped ice[a]	218	1.0×10^{-6}	>0.1
	228	1.0×10^{-6}	>0.1
$ClONO_2$ + HCl on HNO_3-doped ice	218	1.0×10^{-7}	0.023 ± 0.012
	218	1.9×10^{-7}	0.037 ± 0.010
	218	2.0×10^{-7}	0.048 ± 0.018
	218	3.8×10^{-7}	0.058 ± 0.021
	218	4.0×10^{-7}	0.057 ± 0.020
	218	4.1×10^{-7}	0.049 ± 0.015
	218	6.0×10^{-7}	0.072 ± 0.021
	218	6.1×10^{-7}	0.078 ± 0.025
	228	4.4×10^{-7}	0.020 ± 0.0045
	228	5.0×10^{-7}	0.023 ± 0.0081
	228	6.6×10^{-7}	0.025 ± 0.010
	228	7.6×10^{-7}	0.027 ± 0.0071
	228	8.8×10^{-7}	0.036 ± 0.0084
	228	1.0×10^{-6}	0.033 ± 0.0050
	228	1.1×10^{-6}	0.0040 ± 0.0068

[a] $P_{ClONO_2} = 5.0 \times 10^{-7}$ Torr.

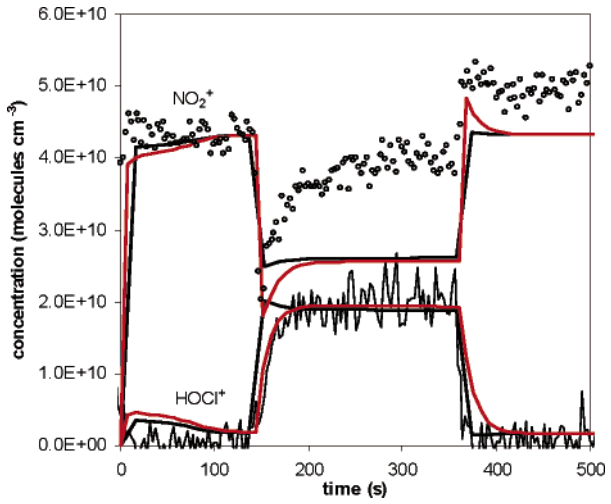

Figure 4. Uptake of $ClONO_2$ ($P_{ClONO_2} \sim 7.0 \times 10^{-7}$ Torr) on HNO_3-doped ice at 218 K. HNO_3-doped ice was exposed to $ClONO_2$ at $t =$ 140 s and stopped at $t = 370$ s. NO_2^+ is shown by empty circles and $HOCl^+$ is represented by the noisy black line. The NO_2^+ signal has been offset by $+1 \times 10^{10}$ molecules cm^{-3} for clarity. The solid line fits to the data represent model simulations for $ClONO_2$ and HOCl gas-phase concentrations with Eley−Rideal (black line) and Langmuir−Hinshelwood (red line) surface reaction mechanisms.

maximum production rate until ~60 s after exposure. The fact that the HOCl signal dropped rapidly when exposure stopped suggests that HOCl is not significantly adsorbed on HNO_3-doped ice at this temperature. We propose that the delay (~60 s) in the HOCl signal is due to build up of sufficient $ClONO_2$ on the surface to obtain the maximum rate of surface reaction. Since the surface was initially saturated with HNO_3 molecules, any HNO_3 formed from $ClONO_2$ hydrolysis could have desorbed immediately upon exposure of $ClONO_2$ to the surface. This desorption precludes any quantitative analysis of the $ClONO_2$

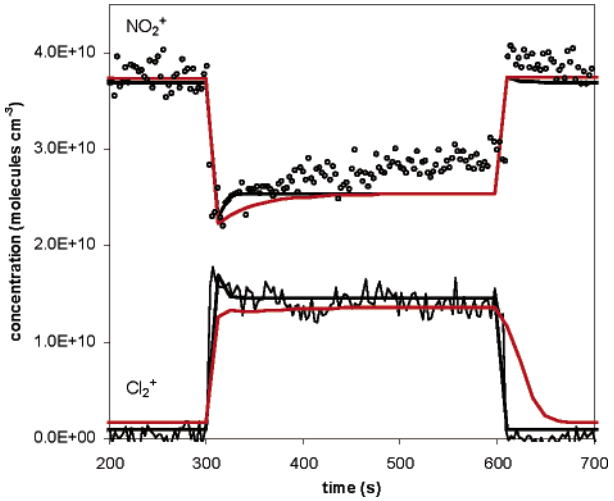

Figure 5. $ClONO_2$ uptake on HCl-doped ice at 218 K. Empty circles represent the NO_2^+ signal and the noisy black line the $HOCl^+$ signal. The NO_2^+ signal has been offset by $+1 \times 10^{10}$ molecules cm^{-3} for clarity. Ice was exposed to the $ClONO_2$ gas stream at $t = 300$ s and exposure stopped at $t = 600$ s. The solid line fits to the data represent model simulations for $ClONO_2$ and HOCl gas-phase concentrations with Eley−Rideal (black line) and Langmuir−Hinshelwood (red line) surface reaction mechanisms.

time dependence from the NO_2^+ signal. This is supported by the observation that the total HOCl produced was much larger than the apparent $ClONO_2$ lost. However, kinetic information can be obtained from the product signal and hence a reactive uptake coefficient for $ClONO_2$ can be determined from the magnitude of the $HOCl^+$ signal. Using this method of analysis, γ_{max} for $ClONO_2$ on HNO_3-doped ice was 0.019 ± 0.006 at 218 K and 0.009 ± 0.004 at 228 K. At 218 K this compares well with the steady-state uptake coefficient on bare ice at $P_{ClONO_2} \sim 7 \times 10^{-7}$ Torr of $\gamma_{ss} = 0.02$, when the surface was likely to be almost saturated with HNO_3 molecules formed from the hydrolysis reaction. These uptake coefficients are summarized in Table 2.

$ClONO_2$ Reactive Uptake on HCl-Doped and HCl/HNO_3-Doped Ice. Experiments were conducted to investigate the reactivity of $ClONO_2$ with adsorbed HCl at 218 K. The ice surface was continuously exposed to 1×10^{-6} Torr of HCl until a saturated surface coverage of HCl was achieved. The surface coverage of HCl for these conditions was $\sim 2.0 \times 10^{14}$ molecules cm^{-2}.[35] Figure 5 shows an uptake experiment for $ClONO_2$ on HCl-doped ice. HCl-doped ice was exposed to $ClONO_2$ between $t = 300$ and 600 s. The smooth lines are numerical model fits to the experimental data discussed later. Rapid uptake of $ClONO_2$ was observed on the surface with $\gamma_{max} > 0.1$. The rate of uptake was diffusion limited so only lower limits to the uptake coefficient could be determined. Cl_2 was instantaneously detected in the gas phase upon exposure of $ClONO_2$ to the surface with no detectable gas-phase HOCl. The rate of Cl_2 formation reached a maximum immediately after $ClONO_2$ exposure and then settled to a constant steady production rate. It is concluded that $ClONO_2$ reacts very quickly on an HCl-doped ice surface to form Cl_2 with a 1:1 stoichiometry. The slight fall off in the maximum uptake rate is probably due to reduction of the HCl surface coverage resulting from the fast reaction and HNO_3 production. This is supported by the observed simultaneous loss of gas-phase HCl to the surface.

A further set of experiments was carried out to probe the $ClONO_2$ reactivity to HCl-doped ice at lower surface concentrations of HCl. To reduce the concentration of surface HCl and

in turn the rate of $ClONO_2$ processing, the ice surface was continually doped with HNO_3 ($P_{HNO3} = 1.0 \times 10^{-6}$ Torr). Once a saturated surface coverage of HNO_3 had been attained, HCl was introduced ($P_{HCl} = (1-10) \times 10^{-7}$ Torr) to the gas stream at the upstream end of the flow tube such that the entire surface of ice was then doped with HCl. The surface coverage of HCl on this HNO_3-doped surface was calculated by using the isotherms in Figure 2a−c. Both HNO_3 and HCl gas flows were kept constant throughout the entire duration of these experiments. Once an equilibrium surface coverage of HCl had been attained, typically after approximately 1 h, a $ClONO_2$ flow was established via the sliding injector. Once all signals were stable, the injector was pulled back to expose a known length of doped ice to the $ClONO_2$ gas stream.

Parts a and b of Figure 6 show $ClONO_2$ uptakes on HCl/HNO_3-doped ice under two scenarios: (a) $P_{HCl} > P_{ClONO_2}$ and (b) $P_{HCl} < P_{ClONO_2}$. The initial HCl surface concentration in Figure 6a was 1.8×10^{13} molecules cm^{-2} ($P_{HCl} = 6.1 \times 10^{-7}$ Torr), and that in Figure 6b was 6.1×10^{12} molecules cm^{-2} ($P_{HCl} = 2.1 \times 10^{-7}$ Torr). In both cases P_{HCl}, and hence HCl coverage, declined following exposure to $ClONO_2$. The NO_2^+ signal decreased sharply in both cases when the sliding injector was pulled back to expose the ice surface. The time dependence in the NO_2^+ signal (in both figures) reflected both $ClONO_2$ loss and HNO_3 desorption from the surface as previously discussed. Since some HNO_3 molecules may desorb, the initial drop in the NO_2^+ signal should represent a lower limit for the maximum uptake, although the effect will be mitigated by the release of sites occupied by HCl, and may allow some HNO_3 produced to remain adsorbed.

The "true" $ClONO_2$ signal in Figure 6a should mirror the Cl_2 production trace that was used to calculate γ_{max} and eliminate the uncertainty introduced by HNO_3 desorption. It was found that γ_{max} values for $ClONO_2$ calculated with use of the NO_2^+ signal were very similar to those calculated from the Cl_2^+ signal suggesting that initially, HNO_3 remains adsorbed on the ice surface. Following this maximum uptake, the rate of reaction depends on a balance between the rate of HCl replenishment at the surface, the $ClONO_2$ flux to the surface, and the reaction rate. Both HCl and $ClONO_2$ compete for adsorption at the surface. The slow decrease in the gas-phase HCl concentration to a new constant value is consistent with the establishment of a new surface equilibrium. Experiments have been carried out at 218 and 228 K with $P_{HCl} = (0.2-1.0) \times 10^{-6}$ Torr.

Figure 6b ($P_{HCl} < P_{ClONO_2}$) shows somewhat different behavior from Figure 6a with both Cl_2 and HOCl liberated to the gas phase. During the uptake, the Cl_2 production rate goes through a sharp maximum on exposure of $ClONO_2$ before falling to a constant value. During this time, HOCl production reaches a maximum value and remains constant until the exposure of the ice surface to the $ClONO_2$ flow is stopped. Evidently at this low HCl surface coverage and low P_{HCl} there is a competition between $ClONO_2$ reacting with H_2O and HCl (reactions R1 and R2). The same behavior was observed at 228 K when $P_{HCl} < P_{ClONO_2}$.

Analysis of the data from the steady-state region of the uptake experiments is complicated by the uncertainty in the surface coverage of HCl, which changes from the initial coverage to a steady-state value as the reaction proceeds. In this steady-state region the HCl surface concentration depends on the reactive processing rate and the replenishment rate from the gas phase. Furthermore, under conditions where there is a competition between reactions R1 and R2 (Figure 6b), uncertainty in the surface concentration of both HCl and H_2O during the steady state complicates any quantitative analysis of these data. Taking the HCl signal level during steady state uptake and predicting the surface coverages from Figure 2 results in coverages which are far too large to result in the smaller uptake coefficients measured. It is suggested that the reactive processing at the surface is sufficiently fast that uptake of gas-phase HCl becomes rate limiting and the surface concentration of HCl is reduced below the Langmuir equilibrium surface coverage. The HCl surface replenishment rate is governed by competitive adsorption of $ClONO_2$, HCl, and HNO_3 on the HNO_3-doped ice. The γ_{ss} of HCl in the two uptake experiments in parts a and b of Figure 6 were calculated from the drop in the HCl signal and found to

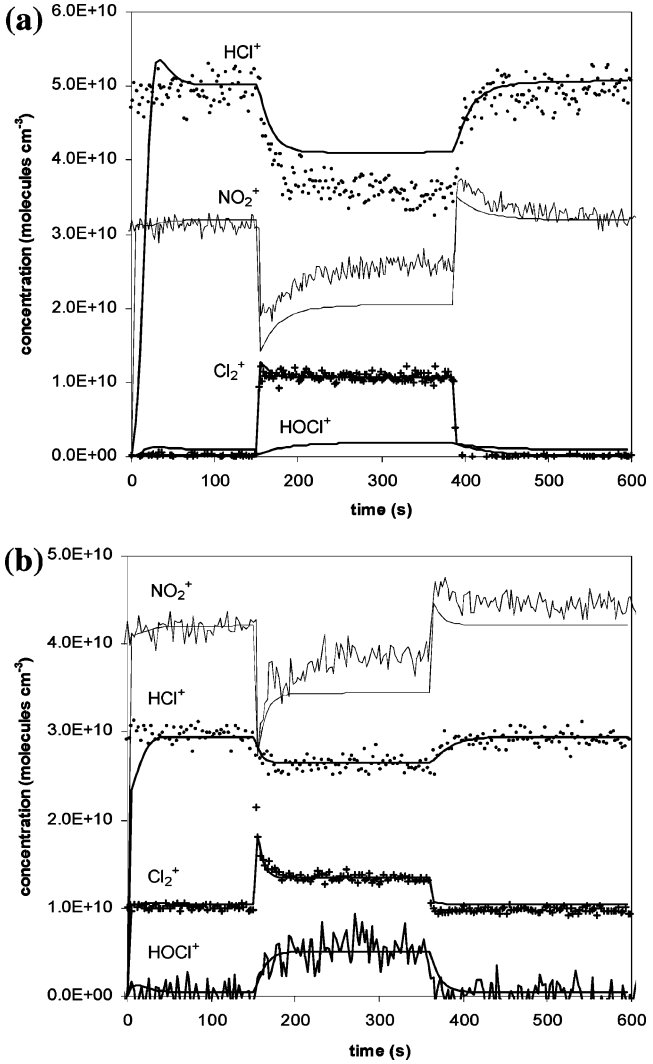

Figure 6. $ClONO_2$ uptake experiments on ice surfaces doped with HNO_3 and HCl at 218 K. (a) $P_{HCl} > P_{ClONO_2}$ with an HCl surface concentration of 1.8×10^{13} molecules cm^{-2}. $ClONO_2$ exposure to the ice surface starts at $t = 150$ s and stops at $t = 390$ s. Under these conditions Cl_2 is the only product detected. (b) $P_{HCl} < P_{ClONO_2}$ with an HCl surface concentration of 6.1×10^{12} molecules cm^{-2}. $ClONO_2$ exposure to the ice surface starts at $t = 150$ s and stops at $t = 370$ s. Both Cl_2 and HOCl are detected as products. The HCl^+ and NO_2^+ signals have been offset by $+2 \times 10^{10}$ molecules cm^{-3} and the Cl_2 signal offset by $+1 \times 10^{10}$ molecules cm^{-3} for clarity. Solid lines in both figures are model fits to the experimental data. The smooth line fit to the NO_2^+ experimental data represents the model simulation of the $ClONO_2$ gas-phase concentration only and not the combined contributions of $ClONO_2$ + HNO_3. The hydrolysis reaction was modeled with a Langmuir−Hinshelwood surface reaction mechanism while reaction with HCl was modeled with an Eley−Rideal mechanism.

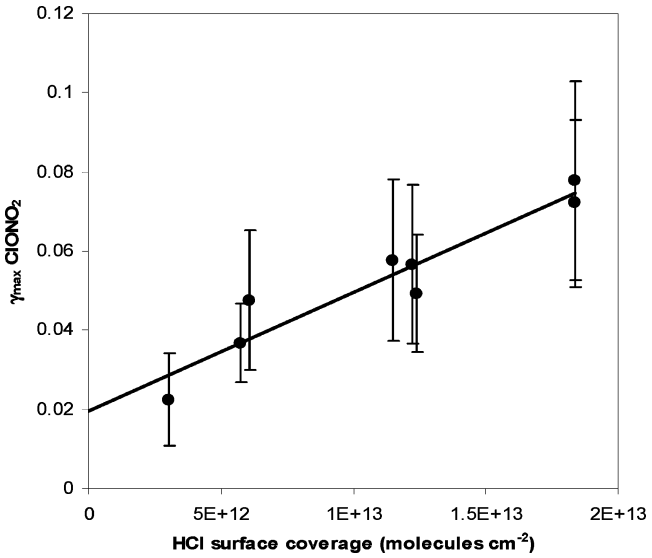

Figure 7. $ClONO_2$ maximum uptake coefficient dependence on HCl surface coverage on HNO_3-doped ice at 218 K.

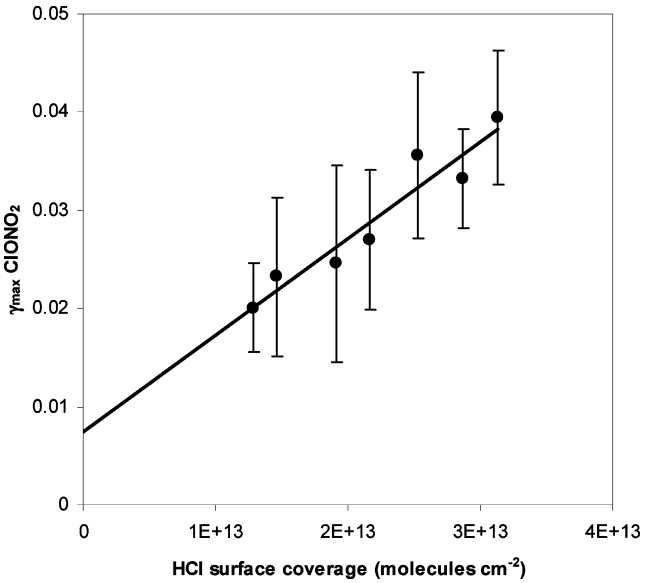

Figure 8. $ClONO_2$ maximum uptake coefficient dependence on HCl surface coverage on HNO_3-doped ice at 228 K.

be 0.005 and 0.004, respectively. For comparison, γ_{ss} of $ClONO_2$ during this period were calculated from the Cl_2 signal and, in the case of Figure 6b, the Cl_2 and HOCl signals. The values were 0.05 and 0.01, respectively. Hence the uptake coefficient of $ClONO_2$ on the doped ice surface was apparently higher than that for uptake of HCl. When $P_{ClONO_2} < P_{HCl}$, there was sufficient gas-phase HCl to maintain a flux of HCl sufficient to support a constant reaction rate and make Cl_2 formation dominant over the hydrolysis reaction. When $P_{ClONO_2} > P_{HCl}$, the gas-phase HCl concentration was insufficient to maintain a high enough flux to the surface to maintain reaction R2 and surface adsorbed $ClONO_2$ undergoes hydrolysis to form HOCl. The continuous production of Cl_2 may reflect HCl impinging on a partially $ClONO_2$-doped surface, which arises as a result of the slower reaction rate of reaction R1 compared with reaction R2. The availability of surface water molecules is likely to be affected by the presence of adsorbed HNO_3 and HCl on the surface.[36] Despite the uncertainties which preclude any quantitative analysis of these data it is clear that at the lowest surface coverages of HCl and when $P_{ClONO_2} > P_{HCl}$, there exists a competition between reaction R1 and reaction R2 such that both Cl_2 and HOCl are liberated to the gas phase. This scenario may be the most applicable to the atmosphere where low P_{HCl} will result in low HCl surface coverage, especially in the presence of HNO_3.

Figures 7 and 8 show the dependence of the γ_{max} $ClONO_2$ as a function of initial HCl surface coverage at 218 and 228 K, respectively. These data was obtained under conditions where $P_{HCl} > P_{ClONO_2}$. The solid lines are least squares weighted fits to the data points. The $ClONO_2$ uptake coefficient was found to vary linearly with HCl surface coverage corresponding to the range $P_{HCl} = (1-10) \times 10^{-7}$ Torr and was found to be independent of P_{ClONO_2} in the range $(4-10) \times 10^{-7}$ Torr indicating that any underestimation of γ_{max} due to HCl surface depletion is minimal. The data were adequately fit by straight lines with intercepts of $\gamma_{max} = 0.020 \pm 0.005$ at 218 K and $\gamma_{max} = 0.008 \pm 0.002$ at 228 K. The reaction probabilities at the intercept correspond to the uptake of $ClONO_2$ on HNO_3-doped ice in the absence of HCl. These are in good agreement with independent measurements of these reaction probabilities of $\gamma_{max} = 0.019 \pm 0.006$ at 218 K and $\gamma_{max} = 0.009 \pm 0.004$ at 228 K.

Reaction Mechanism and Modeling

Reaction Mechanisms. To parametrize the $ClONO_2$ reactivity under different atmospherically relevant conditions it is necessary to have knowledge of the reaction mechanism. Although our kinetic data do not provide conclusive proof of the mechanisms it is clear that the hydrolysis reaction and reaction with HCl (reactions R1 and R2) occur via different reaction mechanisms. This conclusion is based on the differences in the HOCl and Cl_2 product profiles.

On bare ice (Figure 3), the rate of HOCl production passes through a maximum before reaching a steady-state value. The point at which the rate of HOCl production becomes constant coincides with the uptake of $\sim 3 \times 10^{14}$ molecules cm^{-2} of $ClONO_2$, which also corresponds to the saturated surface coverage of HNO_3 (the byproduct of reaction R1). It is concluded that adsorbed HNO_3 reduces the availability of surface H_2O molecules for hydrolysis of $ClONO_2$. The HOCl profile in Figure 4 and the observation that γ_{ss} (HOCl from bare ice) $\cong \gamma_{max}$ (HOCl from HNO_3-doped ice) supports this hypothesis. It was also noted that maximum HOCl production from bare and HNO_3-doped ice did not occur instantaneously and instead took $\sim$60 s from the $ClONO_2$ exposure. Given the high propensity for HOCl desorption from ice at these temperatures[31,32] and the rapid initial loss of $ClONO_2$ from the gas phase (see Figure 4 at $t = 140$ s), it is suggested that the delay in HOCl desorption comes from the accumulation of a precursor species, namely surface adsorbed $ClONO_2$. In contrast, Figures 5 and 6 show that Cl_2 production from $ClONO_2$ uptake on ice, which has a saturated surface coverage of HCl, occurs instantaneously within the time response of the experimental system and on the same time scale as $ClONO_2$ loss to the surface. $ClONO_2$ has to compete for sites with HCl (and HNO_3) before it can adsorb and it is likely that the maximum uptake coefficient of $ClONO_2$ will have a major contribution from the direct reaction with surface HCl but also contain a minor contribution from adsorption to H_2O sites, which only yields any detectable HOCl when the surface HCl concentration is low as in Figure 6b. The instant production of Cl_2 is consistent with a direct reaction mechanism (Eley−Rideal). It follows therefore that the results of these experiments do not support the indirect Cl_2 formation pathway for R2 postulated in the literature[5] where $ClONO_2$ first reacts with surface H_2O to produce surface HOCl

which reacts with adsorbed HCl to release Cl_2 to the gas phase. If this reactive pathway were occurring we would expect to see a Cl_2 formation profile from $ClONO_2$ + HCl-doped ice experiments (Figure 5) similar to that in Figure 3 ($ClONO_2$ + H_2O) for hydrolysis where the HOCl formation rate passes through a maximum during the initial stages of the uptake due to coverage of surface sites by strongly adsorbed HNO_3. Instead we see immediate and constant Cl_2 formation in Figure 5.

The conclusions concerning the mechanism are in agreement with those presented by Oppliger et al.[8] based on experiments at lower temperatures (180−200 K) with a Knudsen cell. In the following section, a numerical model is used to simulate the experimental data and to explore further the assignment of reaction mechanisms to reactions R1 and R2.

Model Calculations. To further investigate the kinetics of the heterogeneous reactions occurring in this system we have used a numerical model to simulate the flow and uptake kinetics of trace gases on surfaces in coated wall flow tube experiments. The model uses the FACSIMILE program[37] and is described in detail elsewhere.[30] The main features include transport of gases along the flow tube, interaction of trace species with the surface, simple Langmuir-type uptake, a diffusive process into the subsurface layers of the ice film, and reaction between species at the surface. Here, we have used the model to simulate our experimental data to test the proposed mechanisms for $ClONO_2$ reaction at the ice surface, and to derive rate constants for use in atmospheric models.

The reaction schemes are described below where S is a surface site (number cm^{-2}), $k(n)f$ are the forward rate constants, $k(n)r$ are the reverse rate constants, $ks1$and $ks2$ are the rate constants for the $ClONO_2$ Eley−Rideal reaction with HCl (reaction R8) and H_2O (reaction R9), respectively, and $kh1$ and $kh2$ are the rate constants for the $ClONO_2$ Langmuir−Hinshelwood reaction with HCl (reaction R10) and H_2O (reaction R11), respectively. The details of each study will be discussed separately.

Adsorption of HNO_3, HCl, and $ClONO_2$ on ice:

$$HNO_{3(g)} + S \overset{k_1f,k_1r}{\rightleftharpoons} HNO_{3(ads)} \quad \text{(R3)}$$

$$HCl_{(g)} + S \overset{k_2f,k_2r}{\rightleftharpoons} HCl_{(ads)} \quad \text{(R4)}$$

$$HNO_{3(ads)} \overset{k_3f,k_3r}{\rightleftharpoons} HNO_{3(bulk)} + S \quad \text{(R5)}$$

$$HCl_{(ads)} \overset{k_4f,k_4r}{\rightleftharpoons} HCl_{(bulk)} + S \quad \text{(R6)}$$

$$ClONO_{2(g)} + S \overset{k_5f,k_5r}{\rightleftharpoons} ClONO_{2(ads)} \quad \text{(R7)}$$

$ClONO_2$ reactive uptake on ice:

Eley−Rideal

$$ClONO_{2(g)} + HCl_{(ads)} \xrightarrow{ks1} Cl_{2(g)} + HNO_{3(ads)} \quad \text{(R8)}$$

$$ClONO_{2(g)} + H_2O_{(surf)} \xrightarrow{ks2} HOCl_{(g)} + HNO_{3(ads)} \quad \text{(R9)}$$

Langmuir−Hinshelwood

$$ClONO_{2(ads)} + HCl_{(ads)} \xrightarrow{kh1} Cl_{2(g)} + HNO_{3(ads)} + S \quad \text{(R10)}$$

$$ClONO_{2(ads)} + H_2O_{(surf)} \xrightarrow{kh2} HOCl_{(g)} + HNO_{3(ads)} + S \quad \text{(R11)}$$

HCl Uptake on HNO_3-Doped Ice. The model uses a single site Langmuir adsorption mechanism to describe the competitive uptake of both HNO_3 (reaction R3) and HCl (reaction R4) to the ice surface. The forward and reverse rates of reactions R3, R4, and R7 are determined by using eqs 4 and 5

$$k(n)f = \frac{\gamma\omega}{4S_{init}}\ (cm^3\ molecule^{-1}\ s^{-1}) \quad (4)$$

$$k(n)r = \frac{k(n)f}{K_{eq}}\ (s^{-1}) \quad (5)$$

where $n = 1$, 2 (or 5 for $ClONO_2$ eq (R7)), γ is the uptake coefficient, ω is the molecular speed (cm s^{-1}) of the adsorbing molecule, S_{init} is the initial concentration of surface sites (cm^{-2}) included to reduce the surface concentrations to dimensionless surface coverages, and K_{eq} is the surface equilibrium constant (cm^3 $molecule^{-1}$).

The model includes reversible diffusive transport of surface molecules (HNO_3 and HCl only) into a subsurface layer of thickness F_T shown in reactions R5 and R6. The rate of diffusion is calculated by using eq 6 and is described in terms of the diffusion coefficient in ice (D/cm^2 s^{-1}), diffusion depth parameter (film thickness F_T/cm), and time (t/s). D was assumed to be constant and F_T variable for fitting: $n = 3$ or 4 in eq 6.

$$k(n)f = k(n)r = \frac{1}{F_T}\left(\frac{D}{\pi}\right)^{1/2}\left(\frac{1}{t^{1/2}}\right)(s^{-1}) \quad (6)$$

The solid line in Figure 1 is a model fit to the experimental data for HCl uptake on HNO_3-doped ice at 218 K. The model reproduces the main features and time dependence of the uptake. The equilibrium constants for both HNO_3 and HCl were variables in this model and determined by the best fit of the model output to the experimental data. The equilibrium constants determined from the model fits were in good agreement with those presented in Table 1 from analysis of the data in Figure 2. The K_{eq} values given in Table 1 are approximately an order of magnitude greater than those reported in our earlier experimental work for HNO_3 and HCl uptake on bare ice.[21,35] These experimentally determined values were derived from surface coverage measurements over a range of relatively high reactant partial pressures ($P_{HNO_3/HCl} > 1 \times 10^{-7}$ Torr). The uncertainty in the magnitude of K_{eq} is thought to come from a combination of the following factors: (i) At high HNO_3 partial pressures the desorption of HNO_3, and to a lesser extent HCl, from downstream surfaces within the flow tube have a significant effect on the behavior of the NO_2^+ signal in the initial stages of the adsorption, which results in an underestimation in the total amount of HNO_3 adsorbed. This effect translates into erroneously low equilibrium constants from the surface coverage data. (ii) The criteria used to determine the surface coverage may over- or undercompensate for diffusion to subsurface layers requiring a correction in K_{eq} values reported. (iii) The value of θ_{max} in our earlier report was assumed to be 1×10^{15} molecules cm^{-3} whereas it is now clear that the max surface coverage is $\sim 3 \times 10^{14}$ molecules cm^{-2} for both HNO_3 and HCl.

$ClONO_2$ Uptake on Bare and HNO_3-Doped Ice. The reactive uptake of $ClONO_2$ on bare and HNO_3-doped ice was modeled by using both Langmuir−Hinshelwood (reactions R7 and R11) and Eley−Rideal (reaction R9) mechanisms. In the Eley−Rideal mechanism, a gas-phase $ClONO_2$ molecule is assumed to react on collision at a surface site occupied by a water molecule, with a maximum uptake coefficient (γ_0) on a clean ice surface. The rate of reaction R9 ($ks2$) was calculated by using eq 4. In the Langmuir−Hinshelwood treatment, the

gas-phase $ClONO_2$ first establishes a population of surface adsorbed molecules which react at sites occupied by water molecules.

The solid lines in Figure 3 represent model fits to experimental data for $ClONO_2$ uptake on bare ice with use of an Eley−Rideal mechanism (black line) and a Langmuir−Hinshelwood (red line) mechanism. The main difference between the two models occurs during the initial stages of the uptake. The Eley−Rideal simulation results in an instant maximum production of HOCl before returning to a lower steady signal level. The experimentally observed HOCl production reaches a maximum more slowly and begins to fall only after a few tens of seconds at this maximum production rate. This delay in the formation of HOCl has been observed in previous studies of this reaction.[8,38] In this study, only the Langmuir−Hinshelwood simulation reproduced the delay in the attainment of maximum HOCl production although the time to maximum was still shorter than observed. The model output for $ClONO_2$ only matched the experimental NO_2^+ signal in the first 150 s; subsequently desorption of product HNO_3 also contributed to the NO_2^+ signal. A model simulation of desorbed HNO_3 revealed that sufficient HNO_3 desorption had occurred to account for the difference between the experimental NO_2^+ signal and model $ClONO_2$ trace.

The solid lines in Figure 4 show similar model fits for $ClONO_2$ uptake on HNO_3-doped ice: Eley−Rideal (black line) and Langmuir−Hinshelwood (red line). Again the main differences between the two model outputs occur during the initial stages of the exposure. In this case the Langmuir−Hinshelwood model accurately reproduces the time dependence in the HOCl production while the product formation in the Eley−Rideal model is far too rapid. Under HNO_3-doped ice conditions it is anticipated that HNO_3 desorption from the surface will provide a greater contribution to the NO_2^+ signal than in the bare ice experiments since the surface is already close to saturation. This is reflected in the model outputs which show a much greater difference between the experimental NO_2^+ signal and the model $ClONO_2$ than in the bare ice simulations. The model simulation of HNO_3 showed that sufficient desorption had occurred to account for the differences in the experimental NO_2^+ signal and the model $ClONO_2$.

$ClONO_2$ Reactive Uptake on HCl-Doped and HCl/HNO_3-Doped Ice. Figure 5 shows model fits to the experimental data for uptake of $ClONO_2$ on HCl-doped ice. In this case the Eley−Rideal model (black line) provided a better fit to the NO_2^+ and Cl_2^+ data, particularly between $t = 300$ and 380 s. Departure of the model fit from the NO_2^+ signal after 380 s can be explained by desorption of product HNO_3.

A final set of model calculations were carried out to simulate $ClONO_2$ reactive uptake on HCl/HNO_3-doped ice. HNO_3 and HCl doping were modeled as described by reactions R3−R6. $ClONO_2$ uptake was split into reversible adsorption (reaction R7) and two reactive channels represented by reactions R8 and R11, i.e., reaction with surface adsorbed water molecules (Langmuir−Hinshelwood) and direct reaction with surface adsorbed HCl molecules (Eley−Rideal). The assignment of these reaction mechanisms was based on the model fits for $ClONO_2$ uptake on bare, HNO_3-doped, and HCl-doped ice described above. The rate constants of reactions R7 and R8 were calculated with eqs 4 and 5. The value of *kh2* (reaction R11) was variable with a maximum value of 1×10^{-15} cm^2 s^{-1} $molecule^{-1}$ (kinetic limit for reaction on every 2D encounter).

The solid lines in parts a and b of Figure 6 show the model outputs for $ClONO_2$ uptake on HCl/HNO_3-doped ice at 218 K for $P_{HCl} > P_{ClONO_2}$ and $P_{HCl} < P_{ClONO_2}$, respectively. When $P_{HCl} > P_{ClONO_2}$, Cl_2 was the only product detected in the gas phase. The model reproduces the time dependence and magnitude of the Cl_2 production on exposure of the ice film to $ClONO_2$. The model predicts the formation of a small amount ($\sim 2 \times 10^9$ molecules cm^{-3}) of HOCl, which was close to the detection limit of our mass spectrometer. The HCl time dependence is adequately reproduced but the magnitude of the HCl loss to the surface is underestimated by the model. The $ClONO_2$ simulations do not reproduce the NO_2^+ signals which are contaminated by HNO_3 desorption. The model simulations do, however, predict desorption of sufficient HNO_3 to account for the difference between the $ClONO_2$ model and NO_2^+ signal.

TABLE 3: Summary of Parameters Used in Model Calculations of $ClONO_2$ Uptake on HCl/HNO_3-Doped Ice[a]

	$P_{HCl} > P_{ClONO_2}$		$P_{HCl} < P_{ClONO_2}$	
	218 K	228 K	218 K	228 K
$K_{eq}(HCl)/cm^3$ $molecule^{-1}$	2×10^{-11}	2×10^{-11}	2×10^{-11}	2×10^{-11}
$K_{eq}(HNO_3)$	1×10^{-10}	1×10^{-10}	1×10^{-10}	1×10^{-10}
$K_{eq}(ClONO_2)$	4×10^{-11}	4×10^{-11}	4×10^{-11}	4×10^{-11}
$\gamma_{max}(HNO_3)$	0.1	0.1	0.1	0.1
$\gamma_{max}(HCl)$	0.08	0.08	0.08	0.04
$\gamma_r(ClONO_2 + HCl)$	0.1	0.1	0.9	0.2
$\gamma_h(ClONO_2 + H_2O)$	0.02	0.02	0.1	0.1
kh/cm^2 s^{-1} $molecule^{-1}$	1×10^{-15}	1×10^{-15}	1×10^{-15}	1×10^{-15}

[a] K_{eq} = equilibrium constant, γ_r = $ClONO_2$ uptake coefficient for reaction with adsorbed HCl, γ_h = $ClONO_2$ uptake coefficient for reaction with adsorbed H_2O, kh = rate constant for surface reaction between adsorbed $ClONO_2$ and adsorbed H_2O (shown as *kh2* in reaction R11).

When $P_{HCl} < P_{ClONO_2}$, there exists a competition between the two reactive channels (reactions R1 and R2) for $ClONO_2$ such that both HOCl and Cl_2 were liberated to the gas phase. The instant production of Cl_2 was well reproduced as was the more "sluggish" HOCl production. The model also reproduced the HCl^+ signal. The difference between the experimental NO_2^+ signal and the modeled $ClONO_2$ could be quantitatively accounted for by HNO_3 desorption.

The experimental observations of adsorption of strong acids (HNO_3 and HCl) have been well reproduced with a simple numerical model incorporating surface adsorption followed by diffusion into subsurface layers. The diffusion parameters used in the model have been described previously.[30] It emerged that model K_{eq} for HNO_3, HCl, and $ClONO_2$ were not strongly temperature dependent between 218 and 228 K with values of $K_{eq}^{HNO_3} \sim 1 \times 10^{-10}$ cm^3 $molecule^{-1}$, $K_{eq}^{HCl} \sim 2 \times 10^{-11}$ $cm^3 molecule^{-1}$, and $K_{eq}^{ClONO_2} \sim 4 \times 10^{-11}$ cm^3 $molecule^{-1}$. This is somewhat unexpected since K_{eq} for HNO_3 and HCl has been shown by experiment to have negative temperature dependence as shown in Table 1.[21,26] The model K_{eq} are somewhat lower than those resulting from the Langmuir fit to the HCl uptake on HNO_3-doped ice data shown in Figure 2. There are no previously reported $K_{eq}^{ClONO_2}$ for comparison with the value reported here. Under conditions where $P_{HCl} < P_{ClONO_2}$, the model uptake coefficients (see Table 3) for $ClONO_2 + HCl$ were $\gamma_r^{218K} = 0.9$ and $\gamma_r^{228K} = 0.2$. These values are in agreement with the uptake coefficients (γ_0) at maximum HCl surface coverage (3×10^{14} molecules cm^{-2}) determined from extrapolation of the data in Figures 7 and 8 which gave $\gamma_0^{218} = 0.9$ ($+0.08$, -0.3) and $\gamma_0^{228} = 0.3 \pm 0.1$

The modeling simulations support the assignment of a Langmuir−Hinshelwood reaction mechanism to the hydrolysis reaction (reaction R1) and an Eley−Rideal mechanism to the reaction with HCl (reaction R2). Table 3 shows a summary of the modeling parameters which best fit the experimental observations for the reaction mechanism assignment given

above. On the basis of the above analysis, we believe that a parametrization based on the assignment of reaction mechanisms, together with the values presented in Table 3, can be used to determine the rates of $ClONO_2$−ice interactions in the Upper Troposphere.

Parametrization of $ClONO_2$ Reactivity on Cirrus Clouds. A parametrization for the rate coefficient of $ClONO_2$ reaction on ice is presented below for $ClONO_2$ hydrolysis and reaction with adsorbed HCl based on parameters derived from experimental results and modeling presented in this work.

$ClONO_2$ + H_2O. Equation 7 shows the mathematical expression for γ in a Langmuir−Hinshlelwood surface reactivity model[24,39]

$$\frac{1}{\gamma} = \frac{1}{S_0} + \frac{\omega_x \sigma_x}{4k_h[H_2O]_s K} \tag{7}$$

where S_0 is the accommodation coefficient (approximated to be ~0.9 from maximum uptake coefficient determination for $ClONO_2$ + HCl), ω_x is the mean thermal velocity of $ClONO_2$ (cm s^{-1}), σ_x is the surface area occupied by one adsorbed molecule (cm^2 $molecule^{-1}$), K is the modified Langmuir constant ($K = K_{eq}/(1 + K_{eq}[ClONO_2]_s)$), K_{eq} is the surface equilibrium constant for $ClONO_2$, $[ClONO_2]_s$ is the gas-phase concentration of $ClONO_2$ in the immediate vicinity of the surface (molecules cm^{-3}), k_h is the second-order surface rate constant for hydrolysis (cm^2 $molecule^{-1}$ s^{-1}), and $[H_2O]_s$ is the surface concentration of H_2O (~1×10^{15} molecules cm^{-2}).[40] Since HNO_3 is ubiquitous in the UT with a high propensity for adsorption to ice, it is important to include the effect of adsorbed HNO_3 on the number of available surface water molecules. In the presence of gas-phase HNO_3, we assume $[H_2O]_s = (1 \times 10^{15}) - [HNO_3]_{ads}$ (i.e., ignoring sites occupied by HCl and other gases). $[HNO_3]_{ads}$ can be calculated by using the classical Langmuir equation for physical adsorption given below:

$$\frac{[HNO_3]_{ads}}{3 \times 10^{14}} = \frac{[HNO_3]_g K_{eq}^{HNO_3}}{1 + [HNO_3]_g K_{eq}^{HNO_3}} \tag{8}$$

where $[HNO_3]_g$ is the gas-phase concentration of HNO_3 (molecules cm^{-3}) and $K_{eq}^{HNO_3}$ is the equilibrium constant of HNO_3 on ice (cm^3 $molecule^{-1}$).

$ClONO_2$ + HCl. The uptake coefficient for $ClONO_2$ on ice in the presence of adsorbed HCl is well described by an Eley−Rideal reaction mechanism. γ can be calculated by using the expression shown in eq 9:

$$\gamma = \gamma_0 \theta_{HCl} \tag{9}$$

where γ_0 is the uptake coefficient at maximum HCl surface coverage. From an extrapolation of experimentally determined γ values at low HCl surface coverage (in Figures 7 and 8) to a saturated surface coverage of 3×10^{14} molecules cm^{-2}, $\gamma_0^{218} = 0.9$ (+0.08, −0.3) and $\gamma_0^{228} = 0.3 \pm 0.1$. θ_{HCl} in eq 9 is the fractional surface coverage of HCl and can be calculated by using the classical Langmuir eq 8. In the presence of HNO_3, a competitive adsorption Langmuir equation (eq 1) describes the surface coverage of HCl.

Equation 9 can be used to predict the maximum reactive uptake coefficient for reaction R2 at any HCl surface coverage. It follows that, assuming a Langmuir adsorption isotherm for HCl on ice, γ_{max} can be predicted for atmospherically relevant P_{HCl}.

$ClONO_2$ Lifetime and Steady-State ClO Production. The lifetime of $ClONO_2$ with respect to reactions R1 and R2 can be estimated by using the parametrization presented above to calculate γ, atmospheric concentrations of the reactants, and eqs 10 and 11 below:

$$k_{het} = \frac{\gamma \omega S}{4V} \tag{10}$$

$$\tau_{het} = \frac{1}{k_{het}} \tag{11}$$

where k_{het} is the pseudo-first-order rate constant (s^{-1}) for heterogeneous loss of $ClONO_2$ to the ice surface in cirrus clouds, γ is the uptake coefficient of $ClONO_2$ calculated with eqs 9 and 7, ω is the mean molecular speed (cm s^{-1}) of $ClONO_2$, S/V is the surface-to-volume ratio of the cirrus cloud (cm^2 cm^{-3}), and τ_{het} is the atmospheric lifetime of $ClONO_2$ with respect to heterogeneous loss on cirrus ice particles.

Assuming maximum reactant mixing ratios of 2 pptv $ClONO_2$, 500 pptv HCl and 1000 pptv HNO_3, we obtain $\gamma^{218}{}_{R1} = 0.1$, $\gamma^{218}{}_{R2} = 0.03$, $\gamma^{228}{}_{R1} = 0.09$, and $\gamma^{228}{}_{R2} = 0.009$. These uptake coefficients have been used together with a typical surface-to-volume ratio of background cirrus clouds (~2×10^{-5} cm^2 cm^{-3})[41] to calculate the lifetime of $ClONO_2$. The lifetime of $ClONO_2$ was calculated to be ~32 min with respect to loss via reaction R1 and ~40 min for loss via reaction R2 in the temperature range 218−228 K.

The photolysis rate of $ClONO_2$ in the UT is approximately 5×10^{-5} s^{-1}, which corresponds to a lifetime of ~6 h.[9,10] The lifetime calculation suggests that reactive uptake on background cirrus can dominate over photolysis as a loss process for $ClONO_2$ in the UT.

The maximum uptake coefficients for $ClONO_2$ were used to calculate the steady-state concentration of ClO by assuming that reactions R12−R15 represent the dominant production and destruction pathways.

$$ClONO_2 + HCl \xrightarrow{k_1} Cl_2 + HNO_3 \tag{R12}$$

$$Cl_2 + h\nu \xrightarrow{J} 2Cl \tag{R13}$$

$$Cl + O_3 \xrightarrow{k_2} ClO + O_2 \tag{R14}$$

$$ClO + NO_2 + M \xrightarrow{k_3} ClONO_2 + M^* \tag{R15}$$

A steady-state analysis was performed assuming that reactions R12 and R15 are the major rate-limiting processes. Equation 12 shows the resulting steady-state expression for [ClO]:

$$[ClO]_{ss} = \frac{k_1[ClONO_2][HCl]_{surf}}{k_3[NO_2][M]} \tag{12}$$

The gas-phase reactant concentrations were as follows: $[ClONO_2] = 1 \times 10^7$ molecules cm^{-3}, $[NO_2] = 6 \times 10^9$ molecules cm^{-3}, and [M] (air) = 9×10^{18} molecules cm^{-3} at 218 K, 200 mbar (~10 km). $[HCl]_{surf}$ is the fractional surface concentration of HCl calculated by using the classical Langmuir eq 8, $K_{eq} = 2.0 \times 10^{-11}$ cm^3 $molecule^{-1}$, and $[HCl] = 3 \times 10^9$ molecules cm^{-3}. The rate constant k_1 (s^{-1}) was calculated by using the expression shown below (eq 13). $k_3 = 2 \times 10^{-12}$ cm^6 $molecule^{-2}$ s^{-1} at 218 K (1.7×10^{-12} cm^6 $molecule^{-2}$ s^{-1} at 228 K):[15]

$$k_1 = \frac{\gamma_0 \omega}{4} S \quad (13)$$

where γ_0 is the maximum uptake coefficient (0.92 at 218 K and 0.32 at 228 K), ω is the mean molecular speed of the gas (cm s^{-1}), and S is the surface area-to-volume ratio of background cirrus.

This analysis resulted in $[ClO]_{ss} = 1 \times 10^7$ molecules cm^{-3} at 218 K (~1 pptv at 200 mbar) and $[ClO]_{ss} = 4 \times 10^6$ molecules cm^{-3} at 228 K (~0.5 pptv at 200 mbar). A similar calculation with hydrolysis of $ClONO_2$ and the subsequent photolysis of the HOCl product as the major source of ClO was performed. This calculation gave $[ClO]_{ss} \sim 4 \times 10^7$ molecules cm^{-3} at both 218 and 228 K (~4 pptv at 200 mbar). Borrmann et al.[13] report airborne observations during descents of the ER-2 aircraft through a cirrus cloud event near the midlatitude tropopause with ClO abundances of 2.7 pptv. At high latitudes, enhanced ClO mixing ratios of 15−20 pptv were observed near the tropopause.[14] The mechanism for maintaining the observed ClO concentrations is unclear and the effects of chemistry and transport both remain possible. The steady-state ClO calculations performed here suggest that chemical chlorine activation can account for the observations at midlatitudes. Given the relative abundances of surface HCl and H_2O on the cirrus particle surface, it is important to note that chlorine activation via $ClONO_2$ hydrolysis (reaction R1) is likely to be more significant for ClO production than reaction with adsorbed HCl (reaction R2). Both reactions R1 and R2 result in the formation of HNO_3, which removes NO_x from the gas phase. This gas-phase denitrification may increase $[ClO]_{ss}$ by reducing the loss rate of ClO (reaction R14).

The results from this study together with the parametrization presented and the values of the important parameters (γ, K_{eq}) in Table 3 need to be incorporated into atmospheric chemistry models and compared with field observations of ClO to decouple the contributions from chemical processing and transportation and to better understand the role of heterogeneous chemistry in chlorine activation by cirrus clouds.

Acknowledgment. The authors would like to thank the E.U. project CUT-ICE (EVK2-CT-1999-00005) for funding this research. M.A.F. acknowledges the support of a N.E.R.C. Ph.D. research studentship.

References and Notes

(1) Tolbert, M. A.; Rossi, M. J.; Malhotra, R.; Golden, D. M. *Science* **1987**, *238*, 1258.
(2) Molina, M. J.; Tso, T.-L.; Molina, L. T.; Wang, F. C.-Y., *Science* **1987**, *238*, 1253.
(3) Hanson, D. R.; Ravishankara, A. R. *J. Geophys. Res., Atmos.* **1991**, *96*, 5081.
(4) Abbatt, J. P. D.; Molina, M. J. *J. Phys. Chem.* **1992**, *96*, 7674.
(5) Chu, L. T.; Leu, M. T.; Keyser, L. F. *J. Phys. Chem.* **1993**, *97*, 12798.
(6) Lee, S. H.; Leard, D. C.; Zhang, R. Y.; Molina, L. T.; Molina, M. J. *Chem. Phys. Lett.* **1999**, *315*, 7.
(7) Leu, M. T.; Moore, S. B.; Keyser, L. F. *J. Phys. Chem.* **1991**, *95*, 7763.
(8) Oppliger, R.; Allanic, A.; Rossi, M. J. *J. Phys. Chem. A* **1997**, *101*, 1903.
(9) Borrmann, S.; Solomon, S.; Dye, J. E.; Luo, B. P. *Geophys. Res. Lett.* **1996**, *23*, 2133.
(10) Solomon, S.; Borrmann, S.; Garcia, R. R.; Portmann, R.; Thomason, L.; Poole, L. R.; Winker, D.; McCormick, M. P. *J. Geophys. Res., Atmos.* **1997**, *102*, 21411.
(11) Reichardt, J.; Ansmann, A.; Serwazi, M.; Weitkamp, C.; Michaelis, W. *Geophys. Res. Lett.* **1996**, *23*, 1929.
(12) Meilinger, S. K.; Karcher, B.; von Kuhlmann, R.; Peter, T. *Geophys. Res. Lett.* **2001**, *28*, 515.
(13) Borrmann, S.; Solomon, S.; Avallone, L.; Toohey, D.; Baumgardner, D. *Geophys. Res. Lett.* **1997**, *24*, 2011.
(14) Thornton, B. F.; Toohey, D. W.; Avallone, L. M.; Harder, H.; Martinez, M.; Simpas, J. B.; Brune, W. H.; Avery, M. A. *J. Geophys. Res., Atmos.* **2003**, *108*, art. no. 8333.
(15) DeMore, W. B.; Sander, S. P.; Golden, D. M.; Hampson, R. F.; Kurylo, M. J.; Howard, C. J.; Ravishankara, A. R.; Kolb, C. E.; Molina, M. J. *Chemical Kinetics and Photochemical data for use in Stratospheric Modeling, Evaluation No. 12*; Jet Propulsion Laboratory: Pasadena, CA, 1997.
(16) Leu, M.-T. *Geophys. Res. Lett.* **1988**, *15*, 17.
(17) Abbatt, J. P. D. *Geophys. Res. Lett.* **1997**, *24*, 1479.
(18) Chaix, L.; Allanic, A.; Rossi, M. J. *J. Phys. Chem. A* **2000**, *104*, 7268.
(19) Chu, L.; Chu, L. T. *J. Phys. Chem. A* **1999**, *103*, 8640.
(20) Chu, L.; Chu, L. T. *J. Phys. Chem. A* **1999**, *103*, 691.
(21) Hynes, R. G.; Fernandez, M. A.; Cox, R. A. *J. Geophys. Res., Atmos.* **2002**, *107*, 4797.
(22) Zondlo, M. A.; Barone, S. B.; Tolbert, M. A. *Geophys. Res. Lett.* **1997**, *24*, 1391.
(23) Tabazadeh, A.; Turco, R. P. *J. Geophys. Res., Atmos.* **1993**, *98*, 12727.
(24) Carslaw, K. S.; Peter, T. *Geophys. Res. Lett.* **1997**, *24*, 1743.
(25) Percival, C. J.; Mossinger, J. C.; Cox, R. A. *Phys. Chem. Chem. Phys.* **1999**, *1*, 4565.
(26) Ullerstam, M.; Thornberry, T.; Abbatt, J. P. D. *Faraday Discuss.* **2005**, *130*, DOI: 10.1039/b417418f.
(27) Hudson, P. K.; Shilling, J. E.; Tolbert, M. A.; Toon, O. B. *J. Phys. Chem. A* **2002**, *106*, 9874.
(28) Sokolov, O.; Abbatt, J. P. D. *J. Phys. Chem. A* **2002**, *106*, 775.
(29) Winkler, A. K.; Holmes, N. S.; Crowley, J. N. *Phys. Chem. Chem. Phys.* **2002**, *4*, 5270.
(30) Cox, R. A.; Fernandez, M. A.; Ullerstam, M.; Abbatt, J. P. D. *Phys. Chem. Chem. Phys.* **2005**. Submitted for publication.
(31) Chu, L.; Diao, G. W.; Chu, L. T. *J. Phys. Chem. A* **2000**, *104*, 3150.
(32) Horn, A. B.; Sodeau, J. R.; Roddis, T. B.; Williams, N. A. *J. Chem. Soc., Faraday Trans.* **1998**, *94*, 1721.
(33) Brown, R. L. *J. Res. Natl. Bur. Stand.* (*U.S.*) **1978**, *83*, 1.
(34) Sherwood, R. C. R. a. T. C. *The Properties of Gases and Liquids*, 3rd ed.; McGraw-Hill: New York, 1958.
(35) Hynes, R. G.; Mossinger, J. C.; Cox, R. A. *Geophys. Res. Lett.* **2001**, *28*, 2827.
(36) Delval, C.; Fluckiger, B.; Rossi, M. J. *Atmos. Chem. Phys.* **2003**, *3*, 1131.
(37) Curtis, A. R.; Sweetenham, W. P. *AERE Harwell Publication R 12805* **1987**.
(38) Hanson, D. R.; Ravishankara, A. R. *J. Phys. Chem.* **1992**, *96*, 2682.
(39) Ammann, M.; Poschl, U.; Rudich, Y. *Phys. Chem. Chem. Phys.s* **2003**, *5*, 351.
(40) Haynes, D. R.; Tro, N. J.; George, S. M. *J. Phys. Chem.* **1992**, *96*, 8502.
(41) Tabazadeh, A.; Toon, O. B.; Jensen, E. J. *Geophys. Res. Lett.* **1999**, *26*, 2211.